Scripta Materialia 117 (2016) 1–5

Contents lists available at ScienceDirect

Scripta Materialia

journal homepage: www.elsevier.com/locate/scriptamat

Microstructure and texture evolution in aluminum and commercially pure titanium dissimilar welds fabricated using ultrasonic additive manufacturing

Niyanth Sridharan [a,*], Paul Wolcott [b], Marcelo Dapino [b], S.S. Babu [a]

[a] Department of Mechanical, Aerospace, and Biomedical Engineering, University of Tennessee, Knoxville, TN 37996, USA
[b] Department of Mechanical and Aerospace Engineering, The Ohio State University, Columbus, OH 43210, USA

ARTICLE INFO

Article history:
Received 1 December 2015
Received in revised form 9 February 2016
Accepted 9 February 2016
Available online 27 February 2016

Keywords:
UAM
Dissimilar metal weld
EBSD
Texture

ABSTRACT

Ultrasonic additive manufacturing (UAM) is a solid-state hybrid manufacturing technique. In this work characterization using electron back scatter diffraction was performed on aluminum–titanium dissimilar metal welds made using a 9 kW ultrasonic additive manufacturing system. The results showed that the aluminum texture at the interface after ultrasonic additive manufacturing is similar to aluminum texture observed during accumulative roll bonding of aluminum alloys. It is finally concluded that the underlying mechanism of bond formation in ultrasonic additive manufacturing primarily relies on severe shear deformation at the interface.

1. Introduction

Ultrasonic additive manufacturing (UAM) is a solid state fabrication process that combines ultrasonic welding and layered manufacturing techniques where thin metal foils (~150 μm) are joined on top of each other sequentially to produce a three dimensional part [1]. The process applies shear deformation at the mating interfaces that results in the removal of surface oxides and intimate contact between metallic surfaces which leads to a solid state bond [2]. The process parameters that correlate with the bond strength include ultrasonic oscillation amplitude, applied normal force, travel speed of the sonotrode, sonotrode texture, and substrate preheat temperature [3,4]. Since UAM is a low temperature process, it is attractive for joining dissimilar metals that have a tendency to form intermetallics. As a result, wide range of dissimilar metals had been joined using UAM process including Al–Ti [5–7] Al–Cu [8], Al–Ni, and Steel-Ta.

Although several mechanisms have been attributed for solid-state bonding during UAM, it has been widely recognized that recrystallization at the interface leads to a reduction in the interfacial energy resulting in a bond formation [1,9–12]. However other effects such as adhesion and mechanical interlocking are also equally possible [2]. The initiation of solid-state welds has been associated with a threshold strain below which no bonding occurs. This threshold strain is required to overcome the energy barrier to reorient surface atoms and/or to fracture the surface oxides. The magnitude of the threshold deformation also depends on the crystal structure of the metals being joined. This threshold deformation is higher for close packed hexagonal metals (e.g. Ti) than that for the cubic metals (e.g. Al) due to an increase in the energy barrier (the energy barrier is thought of the energy that needs to be spent to bring the atoms in intimate contact) [13]. Surface roughness also affects the bond formation during ultrasonic additive manufacturing. For example, an increase in the bond strength was observed due to enhanced mechanical interlocking [8] brought about by inducing rougher surfaces to abetting interfaces before UAM processing.

In the past, texture evolution has been used as a tool to rationalize the bond formation mechanism during ultrasonic additive manufacturing [10,11] accumulative roll bonding [14,15], and friction stir welding [16]. For UAM, extensive multiscale characterizations using electron back scattered diffraction (EBSD) and transmission electron microscopy (TEM) have revealed equiaxed grains at the interface with a strong {111}<110> shear texture in Al 3003 and Al 6061 builds [1,11]. Thus, it was concluded that the adiabatic temperature rise during plastic deformation resulted in dynamic recrystallization at the interface resulting in bond formation. Nevertheless, removal of surface oxide layers by the scrubbing action between the foils is the necessary first step to bring the materials into intimate contact with each other. The behavior of surface oxides during UAM is still not well understood, with sporadic evidence for presence of and absence of oxide layers at the bond interface [1,17]. Based on the published results, there is a

* Corresponding author.
E-mail address: niyanth.sridharan@gmail.com (N. Sridharan).

http://dx.doi.org/10.1016/j.scriptamat.2016.02.013
1359-6462/

gap in fundamental understanding of bond formation during dissimilar metal welding using UAM and this gap forms the motivation behind the current research.

Aluminum and titanium are industrially important materials and dissimilar welds are often required. However fusion welding Al and Ti has been reported to be difficult due to the formation of intermetallic compounds at the interface necessitating solid state welding techniques [17]. In the past, UAM has been used to successfully join Al 3003 and CP Ti and post-weld heat treatment techniques have been used to improve the mechanical strength of these bonds [5]. The effect of process parameters on the strength of Ti–Al composite structures has been evaluated using statistical analysis techniques such as analysis of variance (ANOVA) [7]. A detailed microstructural evolution is required to understand the bonding mechanism in dissimilar Al-1100 and CP Ti welds made using 9 kW UAM.

2. Experimental procedure

Bilayers of Al-1100 and CP-Ti both 0.005″ thick were welded onto an Al-6061-T6 substrate. The builds were made using a Fabrisonic SonicLayer 4000 9 kW system equipped with subtractive milling capabilities located at The Ohio State University. The parameters used for fabrication were a weld force of 3500 N, weld speed of 25.4 mm/s, and vibration amplitude of 41.55 μm. During deposition, the substrate was preheated to 93.3 °C as this has been shown to enhance plastic flow, improving bonding. The process parameters were developed based on iterative weld trials, which are discussed in [6]. The parameters do not represent a globally optimal set; though provide viable welds using these materials. The samples were then sectioned for metallographic analysis along the plane of vibration of the sonotrode and mounted. During sectioning, care was taken to ensure adequate coolant flow to maintain interface microstructures. Samples were mounted in epoxy at room temperature and polished using emery paper down to 1200 grit followed by diamond polishing using 6, 3, and 1 μm diamond slurries. A final surface polish using a 0.05-micron colloidal silica suspension was done using a Buehler Vibromet for 4.5 h to remove the deformation zone from previous polishing steps. Optical microscopy was performed in a Leica DM 750P microscope. EBSD was performed on a JEOL 6500 FEG Scanning Electron Microscope (SEM). The analysis used an accelerating voltage of 20 kV, probe current of 4.0 nA, step size of 0.5 μm, and working distance of 17 mm. Data analysis was done using EDAX TSL software.

3. Results and discussions

3.1. Optical microscopy

A schematic of the bilayer arrangement is shown in Fig. 1 (a). In the bilayer arrangement, the Al-1100 foil is in contact with the Al substrate as illustrated in Fig. 1 (b) and marked in the micrograph. Plastic flow is more evident on the top surface of the Ti layer where there are more crests and troughs, as shown in Fig. 1 (b). As shown previously no intermetallic formation was observed as the interface [6]. This occurs due to the contact between the sonotrode and the top surface of the build leading to local "trough" and "crest" formations as shown. Al being the softer of the two materials flows around these contours and hence the interface experiences significant plastic flow. For the remaining sections in this paper, the Ti layer in contact with the sonotrode will be referred to as the sonotrode affected region and the opposite side will be referred to as the smooth surface. The effect of the deformation on the crystallographic grain structure needs to be examined to gain a fundamental understanding of the bond formation mechanism. This was realized using EBSD. A detailed description of this technique and the various methods of analysis can be found elsewhere [18].

3.2. Electron back scatter diffraction

3.2.1. Characterization of original foil microstructure

The microstructure of the original Al-1100 substrate, foils and the CP-Ti foils prior to fabrication were characterized using EBSD. This data will be used to understand how UAM altered the microstructure at the interface of the bonded zone. The microstructure is presented in Fig. 2. Detailed texture analysis was performed to understand the interfacial phenomena occurring in the builds. Characterization of the Al-1100 foils revealed that they were supplied in the cold rolled condition, while the Al 6061 substrate material was supplied in the T6 condition. The initial CP-Ti microstructure shows an equiaxed alpha microstructure. The initial grain sizes before UAM were

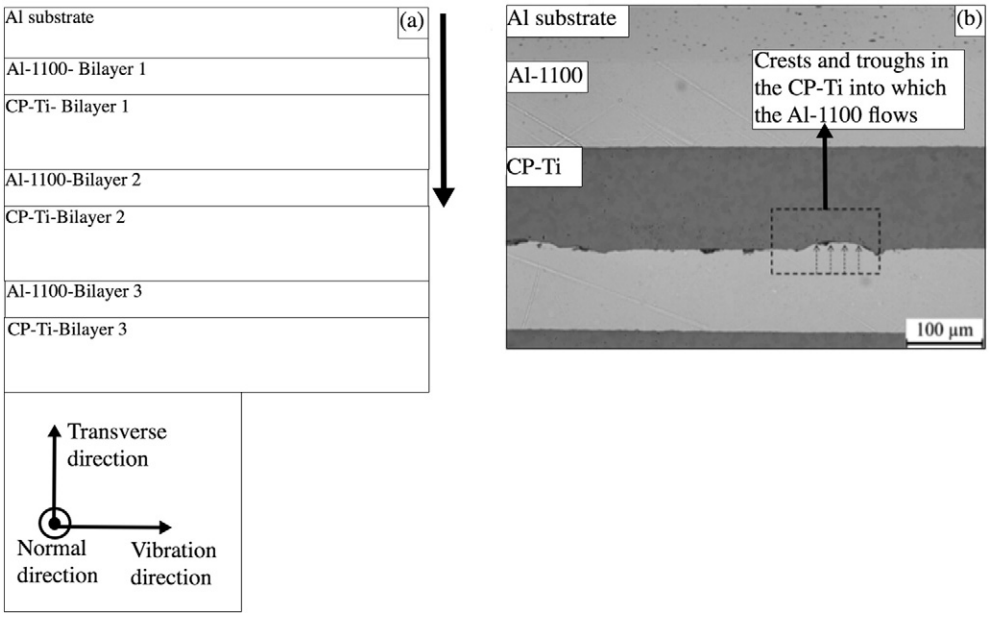

Fig. 1. (a) Showing the schematic of the bilayer arrangement used to fabricate the build. (b) Showing the optical micrograph of the build. The Substrate and the first bilayer. Note the regions where the Al-1100 flowed into the asperities created in the CP-Ti by the sonotrode.

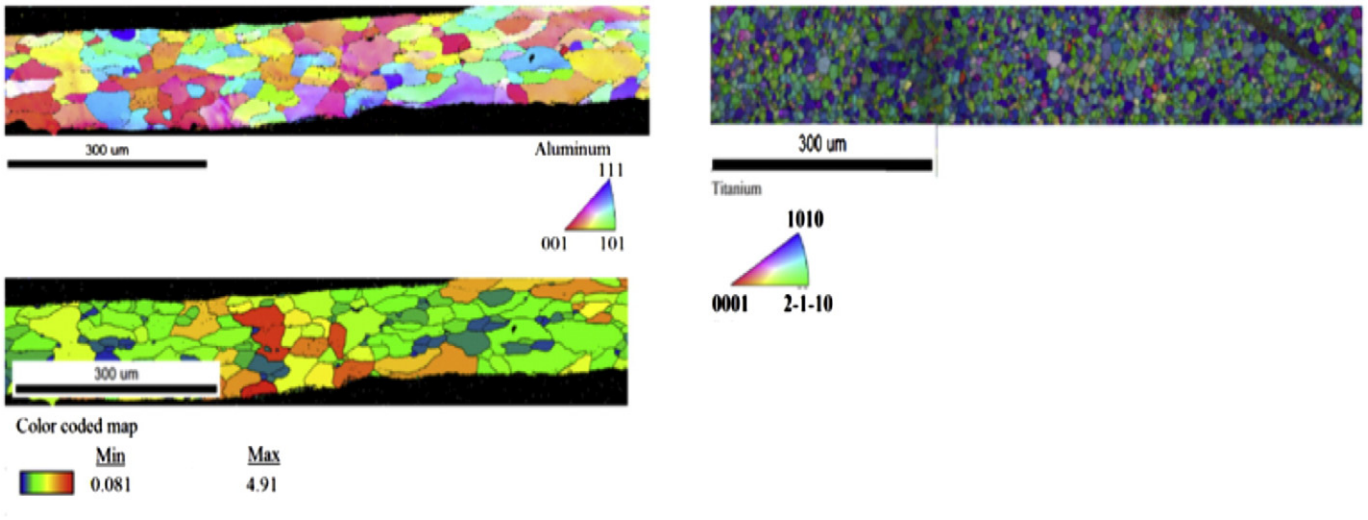

Fig. 2. (a) IPF of as received Al-1100 (b) grain orientation spread of the Al-1100 sample (c) IPF of the as received titanium foil.

17.27 μm and 5.45 μm for the Al-1100 tape and the CP-Ti tape, respectively.

3.2.2. Microstructure evolution at the interfaces

The data from the EBSD measurements were analyzed and the data is shown in Fig. 3. Fig. 3(a) shows the inverse pole figure (IPF) overlaid over the image quality index (IQI). The color coded key for the IPF shows the respective plane normal parallel to the build normal direction. The image quality index (IQI) provides qualitative information about the extent of deformation at the interfaces. Darker regions correspond to heavy deformation and brighter regions correspond to un-deformed or recrystallized regions. The sonotrode-affected regions appear dark in the IQI maps due to the heavy deformation caused by the sonotrode. The titanium side, which is not affected by the sonotrode, on the other hand shows excellent image quality due to the lack of plastic deformation.

It is well known that plastic deformation will lead to an increase in dislocation density contributing to an increase in misorientation within a grain [18]. To quantify this misorientation, the grain orientation spread (GOS) of the grains was analyzed which is shown in Fig. 3(c). It has been reported in the literature that a GOS of <3° corresponds to a completely recrystallized structure [18]. The GOS shows very high misorientations close to 7° in the Al-1100 foils in the middle sections after the UAM processing. However the GOS of the Al-1100 at the interface is less than 3° indicating a recrystallized structure. Thus for all the Al-1100 layers we observe a deformed region sandwiched between the dynamically recrystallized regions as shown in the GOS map. However on analyzing the GOS in the CP-Ti it is observed that there is no appreciable deformation increase except near the sonotrode-affected regions.

3.2.3. Misorientation and grain size distribution

In addition to the GOS, the average grain size and misorientation at each layer was analyzed and the data is presented in Tables 1 through 4. The increase in average misorientation in layer-3 is due to the decrease in the low angle grain boundaries (LABS), which could be an effect of dynamic recrystallization [19]. Previous work on Al-3003 alloys showed that the fraction of HAB's in the bottom layers is higher than the top layers. Experiments where builds were fabricated using embedded thermocouples showed that when the bonding is incomplete in the

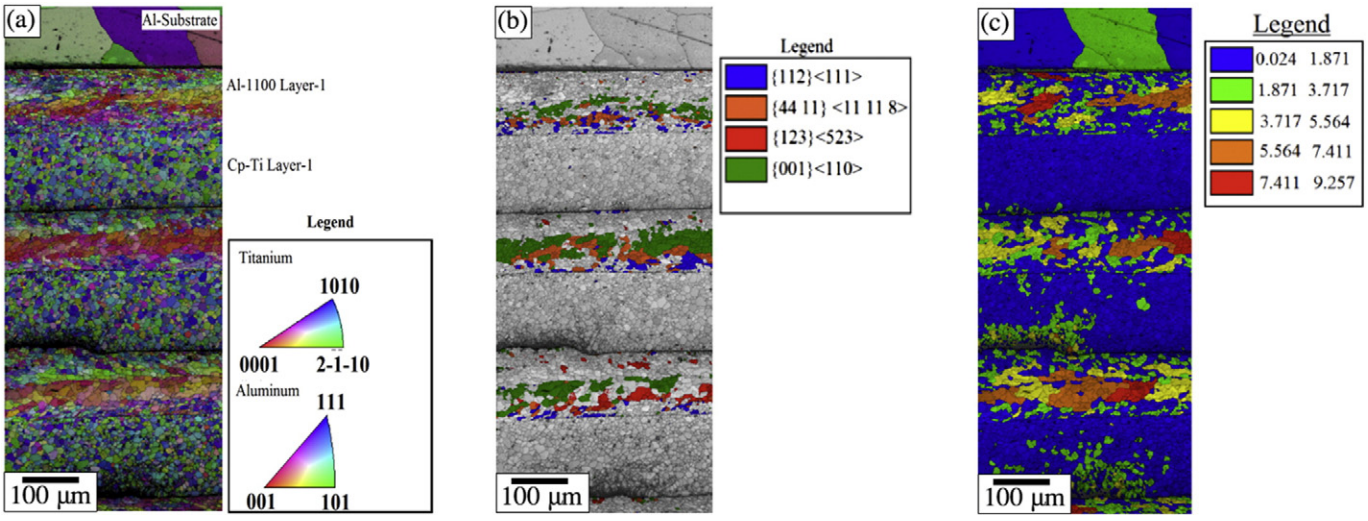

Fig. 3. (a) IPF overlaid with image quality maps showing. (b) Showing the crystal orientations overlaid on an image quality map. (c) Shows the grain orientation spread.

Table 1
Average grain size in the CP-Ti.

Layer	Grain size (μm)
As received	17.27 μm
Layer-1	7.24 μm
Layer-2	8.2 μm
Layer-3	7.3 μm

Table 3
Average misorientation in Al-1100.

Layer	Misorientation
Layer-1	23.14°
Layer-2	22.98°
Layer-3	26.45°

(n − 1)th layer, then on deposition of the nth layer the (n − 1)th layer experiences a spontaneous rise in temperature [20]. This temperature rise is due to the adiabatic heating at the interfaces due to the high strain rate deformation of the tapes at locations where bonding is incomplete. This rise in temperature results in an increase in the fraction of high angle grain boundaries (HAB's) in the (n − 1)th layer and has been observed in Al-3003 [10]. However we don't observe such changes in the fraction of HAB's between the n − 1th and the nth Al-1100 layer. This could be interpreted as complete bonding between the Al-1100-CP-Ti and consequently no temperature rise resulting from the relative motion of the foils. The reason for the increased HAB fraction in layer-3 could be attributed to the additional deformation that the layer-3 underwent. The surface of the Ti in the previous bilayer was roughened due to the pressure created by the sonotrode and had significant surface roughness. Al while flowing around these rough contours had to undergo enhanced plastic deformation due to the roughness of the previous Ti foil that one can see in Fig. 3. This enhanced plastic deformation could have caused a rise in the high angle grain boundary in the Al-1100 in layer 3.

3.2.4. On the evolution of microtexture at the interface

To analyze the nature of the deformation and dynamic recrystallization process, the crystallographic texture was analyzed. For cubic crystals, the texture is represented by {*hkl*} <*uvw*> where {*hkl*} represents the plane parallel to the normal direction of the build and the <*uvw*> represents the crystal direction parallel to the direction of vibration of the build. The crystallographic texture of three layers of Al-1100 is presented in the form of a pole figure in Fig. 4. The rolling texture present in the original aluminum foils changed to the rotated cube texture where {100} ||ND and <110> ||RD. This is the most dominant component at the interface of all these three layers. However there is distinct spread in the orientation in layer-3 as shown in Fig. 4(c). This spread indicates the possibility of developing other texture components during the process. Hence the distribution of various orientations is plotted on the image quality map in Fig. 3(b). From the map it is clear that apart from the rotated cube component which is the major component present, other components such a copper {112} <111> and Dillamore {4 4 11} <11 11 8> were also present at the interfaces. However, these were concentrated only in the region where the Al-1100 came in contact with the relatively smooth surface of the CP-Ti. There is large spread in the orientation where the Al that flowed around the hard Ti asperities. This is indeed a well-known effect where hard particles lead to the development of random orientations at the interface [21].

The copper component is also observed during plane strain rolling of Al alloys to heavy deformation and also during accumulative roll bonding of various Al alloys [14,15]. The strength of the copper texture has been noticed to increase with the number of rolling passes during accumulative roll bonding (ARB), corresponding to an increase in deformation. Apart from the copper texture, the other common texture that has been identified with the accumulative roll bonded Al is the Dillamore texture <4 4 11> <11 11 8> which is just 8° from the copper texture [14]. There are studies that indicate the possibility of forming a strong rotated cube texture {001} <110> type texture at the surface due to the shearing action of the Al sheets when ARB is performed without lubrication [15]. The rotated cube can also rotate to the copper type texture or vice versa by a simple 35° rotation along the transverse direction. The presence of the rotated cube, copper, and Dillamore orientations in the Al foil after UAM shows a similarity with textures developed after ARB. This similarity in texture between UAM and ARB has not been reported earlier. Due to this similarity in the texture it can be concluded that the underlying mechanism of bond formation is similar. There are two criteria to initiate a solid state weld.

i. Removal of surface oxide
ii. Asperity collapse to bring the metals into intimate contact

In the case of ARB (accumulative roll bonding), bonding is achieved by the plastic deformation alone and no macroscopic rise in temperature. The plastic deformation serves to remove the oxide layers and bring nascent metals in intimate contact to achieve a solid-state bond [22]. Since in the case of ARB the mechanical strength increases with the increase in number of passes, it is hypothesized that by increasing the deformation of the foils we may increase the bond strength in UAM also. Troug has previously reported this where he observed an increase in strength when foils with rougher surfaces were used [8].

4. Summary and conclusions

Using electron backscatter diffraction, microstructure and texture evolution of the dissimilar Al–Ti builds fabricated using 9 kW UAM has been investigated. A hypothesis for the bond formation mechanism has been proposed. The results obtained are summarized below:

i. Bond formation occurred without any intermetallic formation.
ii. The deformation is concentrated predominantly in the Al-1100. This has been shown by analyzing the grain sizes where a 10 μm decrease in the Al-1100 grain size after processing occurs whereas the CP-Ti does not show any change in grain size. The grain orientation spread also shows no misorientations in the CP-Ti foils but misorientation increases of up to 9° are observed on the Al side.
iii. As a consequence of the heavy plastic deformation in the Al, the crystallographic texture shows a strong {100} <110> (rotated cube component) with {112} <111> (copper component) and {4 4 11} <11 11 8> (Dillamore component). These texture components also form in Al alloys during ARB.

Table 2
Average grain size in the CP-Ti.

Layer	Grain size (μm)
As received	5.4526
Layer-1	5.3921
Layer-2	5.3214
Layer-3	5.27059

Table 4
Average misorientation in CP-Ti.

Layer	Misorientation
Layer-1	49.8589
Layer-2	44.9578
Layer-3	41.6656

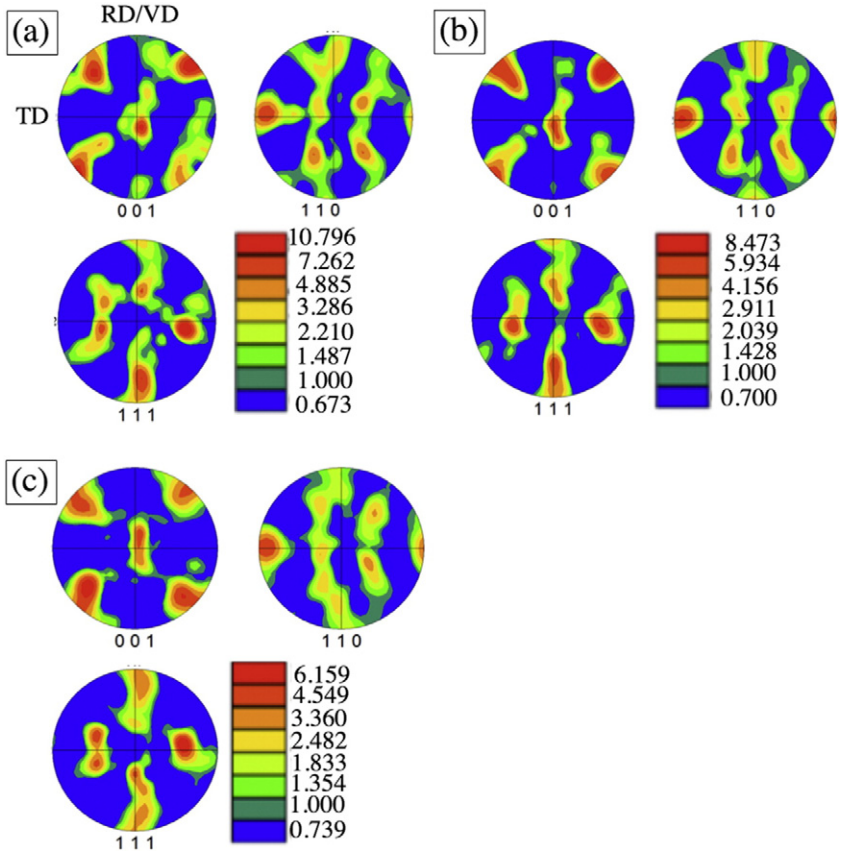

Fig. 4. Texture maps of Al-1100. (a) Layer-1. (b) Layer-2. (c) Layer-3 showing the presence of a strong {001}<110> rotated cube texture.

Based on the very similar texture evolution mechanism in ARB it is proposed that the bonding mechanisms in ARB and UAM rely only on severe plastic deformation. Since both the processes rely on extensive plastic deformation occurring at the interface future work can concentrate on engineering the crystallographic texture of the foils to maximize plastic deformation at the interface.

Acknowledgment

Funding for this work was provided by the Israeli Ministry of Defense (IMOD) under contract number 1000309377. The authors would like to thank Mark Norfolk of Fabrisonic LLC for providing technical support.

References

[1] R. Dehoff, S. Babu, Acta Mater. 58 (2010) 4305–4315.
[2] G.J. Ram, Y. Yang, B. Stucker, J. Manuf. Syst. 25 (2006) 221–238.
[3] C. Kong, R. Soar, P. Dickens, Mater. Sci. Eng. A 363 (2003) 99–106.
[4] C. Kong, R. Soar, P. Dickens, J. Mater. Process. Technol. 146 (2004) 181–187.
[5] J. Obielodan, B. Stucker, E. Martinez, J. Martinez, D. Hernandez, D. Ramirez, L. Murr, J. Mater. Process. Technol. 211 (2011) 988–995.
[6] P. Wolcott, N. Sridharan, S. Babu, A. Miriyev, N. Frage, M. Dapino, Sci. Technol. Weld. Join. (2015) (1362171815Y. 0000000072).
[7] C. Hopkins, M. Dapino, S. Fernandez, J. Eng. Mater. Technol. 132 (2010) 041006.
[8] A.G. Truog, Bond Improvement of Al/Cu Joints Created by Very High Power Ultrasonic Additive Manufacturing, The Ohio State University, 2012.
[9] D. Schick, R. Hahnlen, R. Dehoff, P. Collins, S. Babu, M. Dapino, J. Lippold, Weld. J. 89 (2010) 105S.
[10] H.T. Fujii, M. Sriraman, S. Babu, Metall. Mater. Trans. A 42 (2011) 4045–4055.
[11] S. Shimizu, H. Fujii, Y. Sato, H. Kokawa, M. Sriraman, S. Babu, Acta Mater. 74 (2014) 234–243.
[12] E. Mariani, E. Ghassemieh, Acta Mater. 58 (2010) 2492–2503.
[13] D. Milner, G. Rowe, Metall. Rev. 7 (1962) 433–480.
[14] S. Roy, S. Singh, S. Suwas, S. Kumar, K. Chattopadhyay, Mater. Sci. Eng. A 528 (2011) 8469–8478.
[15] H.W. Kim, S.B. Kang, N. Tsuji, Y.M. Amino, Metall. Mater. Trans. A 36 (2005) 3151–3163.
[16] T. McNelley, S. Swaminathan, J. Su, Scr. Mater. 58 (2008) 349–354.
[17] Y.-C. Kim, A. Fuji, Sci. Technol. Weld. Join. 7 (2002) 149–154.
[18] A.J. Schwartz, M. Kumar, B.L. Adams, D.P. Field, Electron Backscatter Diffraction in Materials Science, Springer, 2009.
[19] T. Sakai, A. Belyakov, R. Kaibyshev, H. Miura, J.J. Jonas, Prog. Mater. Sci. 60 (2014) 130–207.
[20] D. Schick, S. Suresh Babu, D.R. Foster, M. Dapino, M. Short, J.C. Lippold, Rapid Prototyp. J. 17 (2011) 369–379.
[21] K. Lücke, O. Engler, Mater. Sci. Technol. 6 (1990) 1113–1130.
[22] L. Li, K. Nagai, F. Yin, Sci. Technol. Adv. Mater. 9 (2008) 023001.